

# ALLNet: Acute Lymphoblastic Leukemia Detection Using Lightweight Convolutional Networks

Angelo Genovese

Department of Computer Science, Università degli Studi di Milano, 20133 Milano (MI), Italy.

angelo.genovese@unimi.it

**Abstract**—Methods for detecting Acute Lymphoblastic (or Lymphocytic) Leukemia (ALL) based on the analysis of blood images are being increasingly researched in the context of Computer Aided Diagnosis (CAD) systems, which help the pathologist in performing the diagnosis. Within CAD systems, approaches using Deep Learning (DL) and Convolutional Neural Networks (CNN) currently exhibit the highest accuracy in detecting the presence of lymphoblasts, which indicate the possible presence of ALL. Recently, approaches based on histopathological transfer learning have been proposed to increase the accuracy of ALL detection in the presence of databases with a small number of samples, by pretraining the CNN on histopathological data instead of using general-purpose datasets such as ImageNet. However, all the approaches in the literature consider CNN architectures with an extremely high number of learnable parameters, which easily tend to overfit. To compensate for these drawbacks, in this paper we propose ALLNet, the first approach in the literature for ALL detection using a lightweight architecture based on fixed binary kernels that replicate the Local Binary Patterns and that uses only  $\approx 1.6\%$  of the learnable parameters of a traditional CNN. We evaluated our approach on a public ALL database, achieving better results with respect to the state of the art in terms of classification accuracy.

**Index Terms**—Acute Lymphoblastic Leukemia (ALL), Deep Learning (DL), Convolutional Neural Networks (CNN)

## I. INTRODUCTION

Acute Lymphoblastic (or Lymphocytic) Leukemia (ALL) is a disease that affects the blood cells, can spread rapidly throughout the body, and may result in fatal consequences if not detected at an early stage. One of the techniques routinely used to diagnose ALL consists in analyzing White Blood Cells (WBC) present in peripheral blood samples to look for malformations or abnormalities (Fig. 1). Such malformations may be an indicator of lymphoblasts, which naturally occur in the bone marrow. However, an elevated number of WBCs with lymphoblast characteristics may be a sign of ALL [1], [2].

Traditionally, the diagnostic process for detecting ALL is performed manually by an expert pathologist, who looks at the blood cells and estimates the concentration of lymphoblasts present in peripheral blood. Such process, being extremely repetitive and time-consuming, may lead to fatigue, with the consequence that the pathologist could miss important information correlated with the presence of ALL [3].

This work was supported in part by the Italian Ministry of Research within the PRIN program under project HOPE. We thank NVIDIA for the GPU donated.

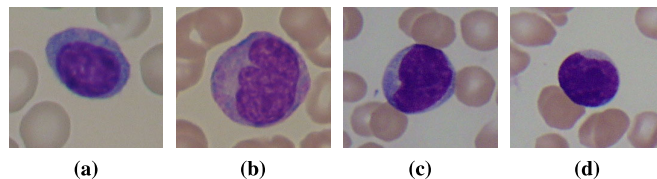


**Fig. 1:** Examples of White Blood Cells (WBC) used to detect the possible presence of Acute Lymphoblastic (or Lymphocytic) Leukemia (ALL): (a,b) “normal” cells; (c,d) “lymphoblasts”.

To overcome the disadvantages of a manual inspection process, Computer Aided Diagnosis (CAD) systems are being increasingly researched: such systems are often based on image processing and machine learning and, by automatically detecting lymphoblasts, can help the pathologist in performing a preliminary screening of the blood samples [4]. Among CAD systems, recent methods are increasingly considering the use of machine learning approaches based on Deep Learning (DL) and Convolutional Neural Networks (CNN), due to their high accuracy in several fields, including medical imaging [5], [6]. In particular, CNNs have the ability of automatically learning data representations, without the need for a handcrafted feature extraction step, with the consequence that CAD systems based on CNNs may be designed with limited knowledge of the application scenario [7].

Currently, the majority of CAD systems based on CNN for the detection of ALL consider the use of transfer learning to increase the classification accuracy, by pretraining the CNN on a larger database (e.g., ImageNet [8]) and then fine tuning it on the ALL database [1], [3], [9]. In fact, while CNNs exhibit high accuracy in several fields, they may not perform optimally in the presence of limited data, as often happens when considering medical records [10], [11].

Recently, instead of using CNNs pretrained on ImageNet, as often happens in computer vision [12], recent DL-based methods for ALL detection consider a CNN pretrained on histopathological data. In fact, histopathological transfer learning proved to increase the classification accuracy by considering a source database more similar to the target database, with respect to a database for generic object detection (such as ImageNet) [3]. However, no method in the literature has yet considered lightweight CNNs for ALL detection with a histopathological transfer learning procedure. Such lightweight

CNNs with a lesser number of learnable parameters have proven to be beneficial in the case of limited data available for training them [13], such as the case of ALL data (e.g., the ALL-IDB database has only 260 images [14]).

In this paper, we propose the first approach in the literature combining lightweight CNNs and histopathological transfer learning for ALL detection, by considering a CNN with fixed kernels that replicate the Local Binary Patterns (LBP)<sup>1</sup>. With respect to the approaches in the literature, our method is able to significantly reduce the number of learnable parameters in the CNNs, limiting overfitting and maintaining a high classification accuracy of WBCs in two classes: *normal* or *lymphoblast*. We evaluate our approach on the Acute Lymphoblastic Leukemia Image Database (ALL-IDB)<sup>2</sup> [14], with results showing a superior accuracy with respect to the literature.

The paper is structured as follows. Section II introduces the relevant literature review. Section III describes the proposed method. Section IV presents the experimental results. Finally, Section V contains the conclusions and future works.

## II. RELATED WORKS

Traditionally, approaches in the literature for ALL detection were divided in methods that considered a handcrafted feature extraction step and methods using only DL [15]. However, recent methods in the literature for medical imaging, histopathology, and ALL detection have been increasingly considering the use of DL and CNNs for their greater accuracy [16], and shifted the attention from the feature extraction step to the design of more efficient learning procedures, novel network architectures, or DL-based preprocessing [1], [3].

When proposing more efficient learning procedures, methods in the literature often consider the use of transfer learning, either by using the ImageNet database to pretrain the CNN [9], [16], [17] or a histopathological database [3]. Then, the methods apply a fine tuning (or deep tuning) step to obtain a CNN able to classify WBCs. In some cases, instead of a tuning phase the methodology considers a feature selection step based on swarm optimization, with the purpose of adapting the pretrained CNNs to blood sample images [18].

When designing innovative network architectures, the approaches may consider convolutional layers specifically designed to enhance the details of blood samples, and that can be added to existing CNNs, for example to exploit also the possibility of using pretrained CNNs [19] (e.g., AlexNet [20]). In alternative, methods in the literature have proposed variations of existing CNN architectures (e.g., ResNet [21]) that better focus on details both at a global and a local scale [22]. When dealing with small datasets and reduce overfitting, some approaches have considered Bayesian CNNs, that can also provide uncertainty estimates [23], or custom CNNs with less convolutional layers [24].

Lastly, when introducing novel DL-based preprocessing, some methods in the literature have considered adaptive and intelligent algorithms based on unsupervised CNNs to enhance the images, while also decorrelating the label from the image quality and reduce possible bias in the database [1].

While some approaches in the literature proposed CNN architectures with less convolutional layers to increase efficiency and reduce overfitting [24], such methods require a custom design and have not been pretrained using a histopathological transfer learning procedure. On the contrary, our method is based on a lightweight CNNs that can be applied on any existing CNN architecture (e.g., ResNet) and that is pretrained on histopathological data.

## III. METHODOLOGY

This Section describes the proposed methodology for ALL detection based on lightweight CNNs. Our approach is based on creating the lightweight CNN by substituting the kernels of an existing CNN architecture (e.g., ResNet) with fixed binary kernels. The binary kernels are chosen as an approximation of the LBP and are combined using learnable weights [13]. Since the binary kernels are fixed, the number of learnable parameters is drastically reduced (a  $9\times$  to  $169\times$  reduction), thus reducing the possibility for the CNN to overfit small datasets. After creating the lightweight CNN, we perform a histopathological transfer learning [3], by pretraining the CNN on a database of histopathological data, replacing the last fully-connected (FC) layer, then fine tuning the resulting CNN on the ALL database. Lastly, we classify each WBC as *normal* or *lymphoblast*.

It is possible to divide the proposed approach in the following steps: A) creation of lightweight CNN; B) histopathological pretraining; C) ALL detection. Fig. 2 shows the outline of the methodology.

### A. Creation of Lightweight CNN

We create the lightweight CNN by considering an existing CNN architecture (e.g., ResNet) and replacing each convolutional layer with a Local Binary Convolutional Module (LBCM) [13]<sup>3</sup>. This module is, in turn, composed by 2 convolutional layers:

- 1) The first layer contains 8 binary kernels with size  $3 \times 3$  and fixed weights. The kernels are designed by having  $-1$  at the central cell and  $1$  in one of the other cells, with each filter having only one cell with  $-1$  (central cell) and only one cell with  $1$ . Such structure of the kernel can replicate the image processing operation performed using LBP, as described in [13]. Fig. 3 shows a graphical representation of the binary kernels.
- 2) The second layer contains 8 kernels with size  $1 \times 1$  and learnable weights, designed to perform a weighted sum of the activation maps resulting after the application of the first layer.

<sup>1</sup>The source code is available at:

<https://iebil.di.unimi.it/cnnALL/index.htm>

<sup>2</sup><https://homes.di.unimi.it/scotti/all>

<sup>3</sup><https://github.com/diczca/lbcnn.pytorch>

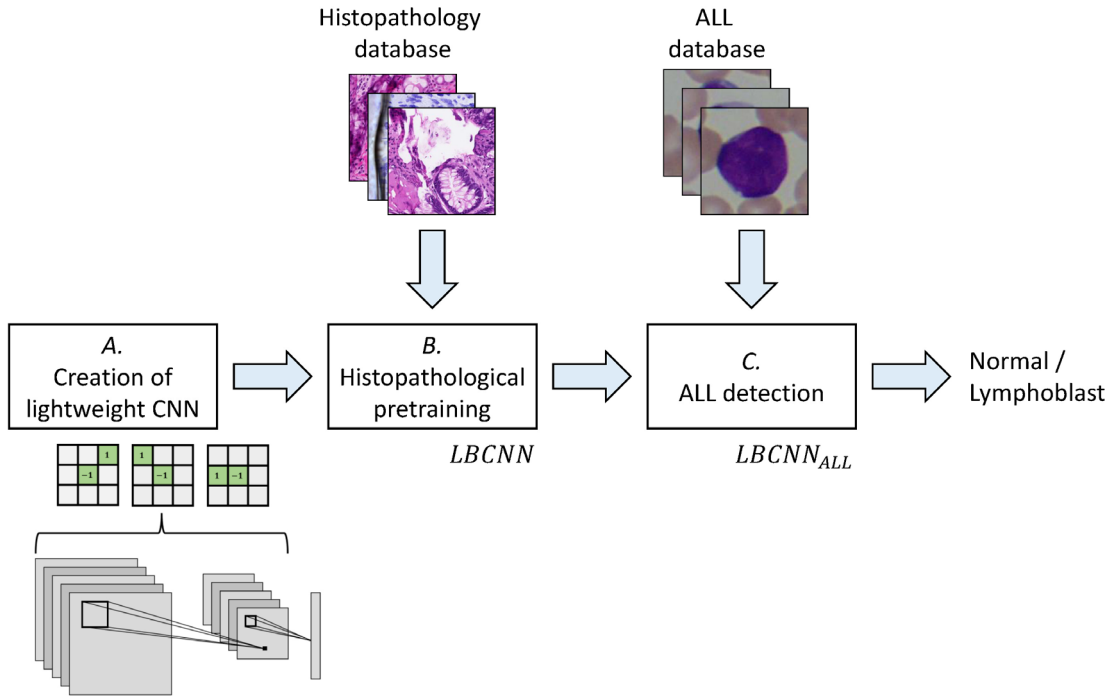


**Fig. 2:** Outline of the proposed methodology. After creating the lightweight CNN using fixed binary kernels (A), we perform a histopathological pretraining (B). Then, we use the resulting CNN to classify each WBC as either *normal* or *lymphoblast* (C).

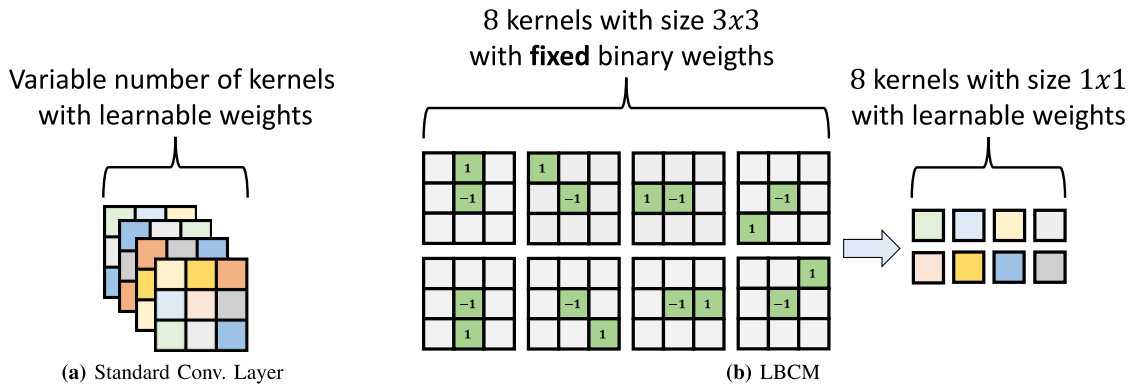


**Fig. 3:** Outline of the Local Binary Convolutional Module (LBCM). In contrast to a standard convolutional layer (a) which contains a variable number of kernels with learnable weights (*colored boxes*), the LBCM (b) contains 8 kernels with size  $3 \times 3$  and fixed binary weights, and only 8 kernels with size  $1 \times 1$  and learnable weights (*colored boxes*).

With respect to a standard convolutional layer, the number of learnable parameters is significantly reduced, since only 8 learnable weights are present for each convolutional layer.

After replacing each convolutional layer of the CNN with a LBCM, we obtain the Local Binary Convolutional Network (LBCNN).

### B. Histopathological Pretraining

To perform the histopathological pretraining, we consider a database containing patches extracted from whole slide imaging samples. Each patch describes a different histological tissue, such as adipose, epithelial, nervous, or skeletal. To facilitate the training process, each patch has its own label.

Since each patch can contain multiple tissues, the labels are not mutually exclusive and each patch usually has multiple labels.

The labeling process for the histopathological database is performed by considering different labeling methodologies, organized in a hierarchical way. In particular, there are  $n$  labeling levels, with each level describing a more precise labeling. Therefore, each patch  $p$  is associated with a set of labels  $L(p) = \{l_i\}_{i=1}^n$ . Since the labeling precision increases with each level,  $l_3$  describes a more precise labeling than  $l_1$ .

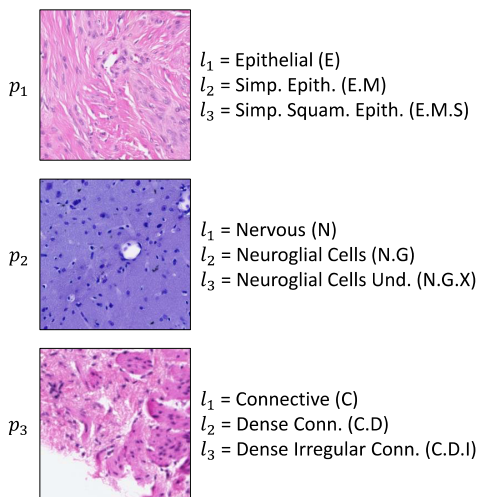


**Fig. 4:** Examples of samples pertaining to the histopathological database. Each sample  $p_i$  has a set of labels associated to it (e.g.,  $l_1$ ,  $l_2$ ,  $l_3$ ), organized in a hierarchical way with each level having a more precise labeling (e.g.,  $l_3$  contains the most precise labeling).

As an example, a patch  $p_i$  can have the following labels:

$$\begin{aligned}
 l_1 &= \text{Nervous (N)} \\
 l_2 &= \text{Neuroglial Cells (N.G)} \\
 l_3 &= \text{Neuroglial Cells Undifferentiated (N.G.X)} \quad (1)
 \end{aligned}$$

Fig. 4 shows examples of patch samples with the associated set of labels.

We train the  $LBCNN$  on the histopathological database to detect in each sample the corresponding histological tissue types, following the training procedures and parameters described in [25] and considering each time a different labeling level. As a result, we obtain  $n$   $LBCNN$ s, one for each of the  $n$  labeling levels:  $\{LBCNN_i\}_{i=1}^n$ .

The only difference in the network architecture among the  $n$   $LBCNN$ s resides in the size of the last FC layer, whose dimension is chosen based on the cardinality of the labeling level. As an example, if there are 1000 possible labels, such as the case for ImageNet, the last FC layer of a CNN trained to classify such database has 1000 neurons. Therefore, each  $LBCNN$  has a last FC layer with size depending on the cardinality of the labeling level. In the considered histopathology database, the cardinality of the first level is  $|\{l_1\}| = 9$ , while the cardinality of the third level, describing a more precise labeling, is  $|\{l_3\}| = 42$ .

### C. ALL Detection

To use the  $LBCNN$ s, pretrained on histopathological data, to perform ALL detection, we apply a transfer learning procedure. First, we replace the last FC layer with a layer whose dimension is suited to the cardinality of the classes in the ALL database. In particular, the ALL database we considered has 2 classes, with each image having a binary label (0: *normal*;

1: *lymphoblast*). Therefore, we replace the last FC layer of each  $\{LBCNN_i\}$  with a FC layer with 2 neurons (Fig. 5).

As a result, we obtain the  $n$  CNNs adapted for ALL detection:  $\{ALLNet_i\}_{i=1}^n$ . Then, we train each  $ALLNet$  by performing a deep tuning on the training subset of the ALL database. In the deep tuning, differently than the fine tuning process, all the weights of the CNN pretrained on the source database are updated when training on the target database. To compensate for the limited number of samples in the ALL database, we perform a data augmentation during the training, by randomly flipping or rotating each image in the training subset.

Lastly, we apply each  $ALLNet$ , pretrained on histopathological data and deep tuned for ALL detection, on the testing subset of the ALL database. The output of the  $ALLNet$  applied on each image is a binary number indicating whether the image is classified as 0: *normal* or as a 1: *lymphoblast*.

## IV. EXPERIMENTAL RESULTS

### A. Used Databases

In the proposed approach, we consider two databases, a source database for histopathological pretraining (see Section III-B) and a target database for ALL detection (see Section III-C).

As the histopathology database, we used the Atlas of Digital Pathology (ADP) [25]<sup>4</sup>, which contains 17,668 RGB image patches  $\{p_i\}$  with size  $272 \times 272$  pixels, extracted from 100 whole slide images. Each patch  $p_i$  is labeled according to  $n = 3$  levels, with each level describing a more precise classification. Moreover, for each level, each patch can have multiple labels, since each patch can describe multiple histological tissues and thus the labels are not mutually exclusive, as described in Section III-B. Examples of images in the ADP database are shown in Fig. 4 along with the corresponding labels.

As the database for ALL detection, we used the ALL-IDB2 database [14]<sup>2</sup>, which contains 260 RGB images of peripheral blood samples with size  $256 \times 256$  pixels, with 130 cells labeled as 0: *normal* and 130 cells labeled as 1: *lymphoblast*.

### B. CNN Training

As mentioned in Section III-A, it is possible to apply the proposed method by considering an existing CNN architecture and modifying it by replacing each convolutional layer with a LBCM. In this work, we considered the ResNet18 and ResNet34 network architectures, since they represent two popular CNN architectures with high accuracy in several fields [13], [21]<sup>5</sup>.

For each chosen architecture, we create the  $LBCNN$  as described in Section III-A and we apply the proposed histopathological pretraining as described in Section III-B. As a result, for each architecture we obtain  $LBCNN_1$ ,  $LBCNN_2$ , and  $LBCNN_3$ , one for each of the  $n = 3$  labeling

<sup>4</sup><https://www.dsp.utoronto.ca/projects/ADP>

<sup>5</sup>More details on the structure of the CNN are available at: <https://iebil.di.unimi.it/cnnALL/index.htm>

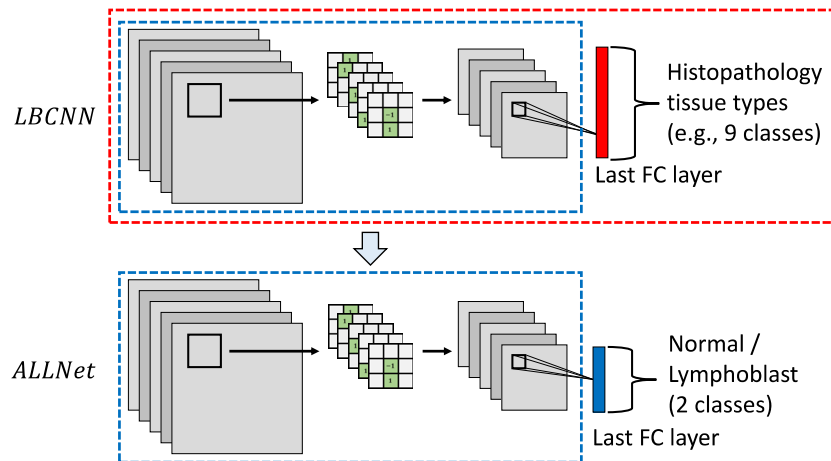


**Fig. 5:** Transfer learning procedure for adapting the *LBCNN*, pretrained on histopathological data, to *ALLNet* for ALL detection. We replace the last FC layer of *LBCNN*, whose dimension is based on the cardinality of the classes in the histopathological data, with a FC layer with 2 neurons.

**TABLE I:** Overview of the different *ALLNets* for ALL detection obtained by applying the proposed method.

		CNN Architecture	
		ResNet18	ResNet34
Level *	1	<i>ALLNet</i> <sub>ResNet18,1</sub>	<i>ALLNet</i> <sub>ResNet34,1</sub>
	2	<i>ALLNet</i> <sub>ResNet18,2</sub>	<i>ALLNet</i> <sub>ResNet34,2</sub>
	3	<i>ALLNet</i> <sub>ResNet18,3</sub>	<i>ALLNet</i> <sub>ResNet34,3</sub>

Notes. \* = Level of histopathology labels (see Section III-B).

levels. To train the *LBCNN*, we apply the parameters and the training procedure described in [3], [25].

To create the *ALLNet*, we apply the procedure described in Section III-C on each pretrained *LBCNN* and we perform the deep tuning on the ALL database. In particular, we obtain an *ALLNet* for each chosen architecture and for each labeling level. A summary of the resulting CNNs is outlined in Table I. To train the *ALLNet*, we split the ALL database as 40% training, 10% validation, and 50% testing. Then, we train each *ALLNet* on the training subset, with a batch size 8 and for 100 epochs, using the Stochastic Gradient Descent (SGD) algorithm. The parameters of the SGD are learning rate  $lr = 0.02$  and momentum  $m = 0.9$ . We half  $lr' = lr/2$  every 20 epochs. After the last epoch, we select the values of the weights for which we obtain the highest classification accuracy on the validation subset. We consider the same training procedure for all the *ALLNets* in Table I.

### C. Evaluation Procedures and Error Measures

To compute the error measures, we perform a  $n$ -fold cross-validation, with  $n = 2$ , repeated 5 times, with the different subsets of the ALL database (training, validation, testing) extracted randomly at each iteration. We compute the error measures on the testing subset. Then, we average the results on the 5 iterations.

The error measures considered in this work are the metrics described in [14], which consist in the mean and standard

**TABLE II:** Accuracy results on the ALL-IDB2 database using the proposed methodology, compared with the literature.

Ref.	Deep CNN	Classification Accuracy (%) (Mean <sub>Std</sub> )
[3]	<i>HistoTNet</i> <sub>ResNet18,1</sub>	95.38 <sub>3.41</sub>
	<i>HistoTNet</i> <sub>ResNet18,2</sub>	97.92 <sub>1.62</sub>
	<i>HistoTNet</i> <sub>ResNet18,3</sub>	97.38 <sub>1.04</sub>
	<i>HistoTNet</i> <sub>ResNet34,1</sub>	97.54 <sub>1.13</sub>
	<i>HistoTNet</i> <sub>ResNet34,2</sub>	96.62 <sub>2.26</sub>
	<i>HistoTNet</i> <sub>ResNet34,3</sub>	97.08 <sub>0.90</sub>
-	<b>ALLNet</b> <sub>ResNet18,1</sub>	<b>97.85</b> <sub>0.58</sub>
	<b>ALLNet</b> <sub>ResNet18,2</sub>	<b>97.54</b> <sub>1.57</sub>
	<b>ALLNet</b> <sub>ResNet18,3</sub>	<b>97.23</b> <sub>2.04</sub>
	<b>ALLNet</b> <sub>ResNet34,1</sub>	<b>95.38</b> <sub>5.01</sub>
	<b>ALLNet</b> <sub>ResNet34,2</sub>	<b>98.46</b> <sub>0.84</sub>
	<b>ALLNet</b> <sub>ResNet34,3</sub>	<b>98.00</b> <sub>1.86</sub>

**TABLE III:** Number of learnable parameters and size of the *ALLNet* used in the proposed methodology and comparison with the literature.

Ref.	Deep CNN	N. of learnable parameters	Size [MB]*
[3]	<i>HistoTNet</i> <sub>ResNet34,2</sub>	21,285,698	83
-	<b>ALLNet</b> <sub>ResNet34,2</sub>	<b>342,082</b>	<b>5</b>

Notes. \*Size computed considering a PyTorch implementation.

deviation of the classification accuracy, as well as the number of true negatives, true positives, false negatives, and false positives.

### D. Accuracy and Complexity

Table II shows the result of each *ALLNet* in terms of classification accuracy, obtained using the proposed methodology. In the Table, we present also the comparison with

**TABLE IV:** Average confusion matrix of the  $ALLNet_{ResNet34,2}$  on the ALL-IDB2 database using the proposed methodology.

		Predicted	
		0 (normal)	1 (lymphoblast)
True	0 (normal)	TN = 49.54%	FP = 0.46%
	1 (lymphoblast)	FN = 1.08%	TP = 48.92%

Notes. TN = True Negatives; TP = True Positives; FN = False Negatives; FP = False Positives.

the accuracy of the  $HistoTNet$  described in [3], which represents the current state of the art. From the Table, it is possible to observe that the proposed method, for each variant of  $ALLNet$ , achieves better or on par accuracy with the literature. In particular,  $ALLNet_{ResNet34,2}$  achieves the best accuracy among the considered variants of  $ALLNet$ . Table IV shows the average confusion matrix obtained using  $ALLNet_{ResNet34,2}$  on the ALL-IDB2 database.

In addition to exhibiting the highest accuracy among the considered CNNs, the  $ALLNet$  considered in the proposed approach use a significantly reduced number of learnable parameters with respect to  $HistoTNet$ , as shown in Table III. In particular, the use of  $ALLNet_{ResNet34,2}$  permits a  $62\times$  reduction in the number of parameters, with the number of learnable parameters in  $ALLNet_{ResNet34,2}$  being 1.61% of the learnable parameters present in  $HistoTNet_{ResNet34,2}$ . Moreover, the table shows how the reduced number of learnable parameters enables to significantly reduce the size of the model and thus save storage space (5 MB instead of 83 MB).

## V. CONCLUSIONS

In this paper we proposed a novel method for Acute Lymphoblastic (or Lymphocytic) Leukemia (ALL) detection based on the analysis of White Blood Cells (WBC) present in peripheral blood. Differently than the methods in the literature, our approach combines a lightweight CNN with a histopathological transfer learning procedure, by introducing a CNN with a reduced number of learnable parameters, that uses fixed kernels that replicate the Local Binary Patterns (LBP) and that is first trained to detect histological tissue types, then tuned on the ALL database to classify each cell as either *normal* or *lymphoblast*. We evaluated our method on a publicly available database designed for ALL detection, with results better than the current state of the art.

## REFERENCES

- [1] A. Genovese, M. S. Hosseini, V. Piuri, K. N. Plataniotis, and F. Scotti, "Acute Lymphoblastic Leukemia detection based on adaptive unsharpening and Deep Learning," in *Proc. of ICASSP*, 2021.
- [2] M. M. Amin, S. Kermani, A. Talebi, and M. G. Oghli, "Recognition of acute lymphoblastic leukemia cells in microscopic images using k-means clustering and support vector machine classifier," *J. Medical Signals Sens.*, vol. 5, no. 1, Jan. 2015.

- [3] A. Genovese, M. S. Hosseini, V. Piuri, K. N. Plataniotis, and F. Scotti, "Histopathological transfer learning for Acute Lymphoblastic Leukemia detection," in *Proc. of CIVEMSA*, 2021.
- [4] H. T. Salah, I. N. Muhsen, M. E. Salama, T. Owaidah, and S. K. Hashmi, "Machine learning applications in the diagnosis of leukemia: Current trends and future directions," *Int. J. Lab. Hematol.*, vol. 41, no. 6, Dec. 2019.
- [5] S. Pouyanfar, S. Sadiq, Y. Yan, H. Tian, Y. Tao, M. P. Reyes, M.-L. Shyu, S.-C. Chen, and S. S. Iyengar, "A survey on deep learning: Algorithms, techniques, and applications," *ACM Comput. Surv.*, vol. 51, no. 5, Sep. 2018.
- [6] S. Kulkarni, N. Seneviratne, M. S. Baig, and A. H. A. Khan, "Artificial intelligence in medicine: Where are we now?" *Acad. Radiol.*, vol. 27, no. 1, Jan. 2020, special Issue: Artificial Intelligence.
- [7] M. Abukmeil, S. Ferrari, A. Genovese, V. Piuri, and F. Scotti, "A survey of unsupervised generative models for exploratory data analysis and representation learning," *ACM Computing Surveys*, 2021.
- [8] O. Russakovsky, J. Deng, H. Su, J. Krause, S. Satheesh, S. Ma, Z. Huang, A. Karpathy, A. Khosla, M. Bernstein, A. C. Berg, and L. Fei-Fei, "ImageNet Large Scale Visual Recognition Challenge," *Int. Journal of Computer Vision*, vol. 115, no. 3, pp. 211–252, 2015.
- [9] S. Shafique and S. Tehsin, "Acute Lymphoblastic Leukemia detection and classification of its subtypes using pretrained Deep Convolutional Neural Networks," *Technol. Cancer Res. T.*, vol. 17, Jan. 2018.
- [10] H. Shin, H. R. Roth, M. Gao, L. Lu, Z. Xu, I. Nogues, J. Yao, D. Mollura, and R. M. Summers, "Deep convolutional neural networks for computer-aided detection: CNN architectures, dataset characteristics and transfer learning," *IEEE Trans. Med. Imag.*, vol. 35, no. 5, pp. 1285–1298, 2016.
- [11] N. Tajbakhsh, J. Y. Shin, S. R. Gurudu, R. T. Hurst, C. B. Kendall, M. B. Gotway, and J. Liang, "Convolutional Neural Networks for medical image analysis: Full training or fine tuning?" *IEEE Trans. on Medical Imaging*, vol. 35, no. 5, pp. 1299–1312, 2016.
- [12] L. Liu, W. Ouyang, X. Wang, P. Fieguth, J. Chen, X. Liu, and M. Pietikäinen, "Deep Learning for generic object detection: A survey," *Int. J. Comput. Vis.*, vol. 128, Feb. 2020.
- [13] F. Juefei-Xu, V. N. Boddeti, and M. Savvides, "Local binary convolutional neural networks," in *Proc. of CVPR*, 2017.
- [14] R. Donida Labati, V. Piuri, and F. Scotti, "ALL-IDB: The Acute Lymphoblastic Leukemia Image Database for image processing," in *Proc. of ICIP*, 2011.
- [15] M. Zolfaghari and H. Sajedi, "A survey on automated detection and classification of acute leukemia and WBCs in microscopic blood cells," *Multimedia Tools and Applications*, 2022.
- [16] A. Loddo and L. Putzu, "On the effectiveness of leukocytes classification methods in a real application scenario," *AI*, vol. 2, no. 3, pp. 394–412, 2021.
- [17] A. Rehman, N. Abbas, T. Saba, S. I. u. Rahman, Z. Mehmood, and H. Kolivand, "Classification of Acute Lymphoblastic Leukemia using Deep Learning," *Microsc. Res. and Tech.*, vol. 81, no. 11, Nov. 2018.
- [18] A. Talaat, P. Kollmannsberger, and A. Ewees, "Efficient classification of white blood cell leukemia with improved swarm optimization of deep features," *Scientific Reports*, vol. 10, no. 2536, Feb. 2020.
- [19] R. Duggal, A. Gupta, R. Gupta, and P. Mallick, "SD-Layer: Stain deconvolutional layer for CNNs in medical microscopic imaging," in *Proc. of MICCAI*, 2017.
- [20] A. Krizhevsky, I. Sutskever, and G. E. Hinton, "ImageNet classification with deep convolutional neural networks," in *Proc. of NIPS*, 2012.
- [21] K. He, X. Zhang, S. Ren, and J. Sun, "Deep residual learning for image recognition," in *Proc. of CVPR*, 2016.
- [22] P. Mathur, M. Piplani, R. Sawhney, A. Jindal, and R. R. Shah, "Mixup multi-attention multi-tasking model for early-stage leukemia identification," in *Proc. of ICASSP*, 2020.
- [23] M. E. Billah and F. Javed, "Bayesian convolutional neural network-based models for diagnosis of blood cancer," *Applied Artificial Intelligence*, pp. 1–22, 2021.
- [24] A. Kumar, J. Rawat, I. Kumar, M. Rashid, K. U. Singh, Y. D. Al-Otaibi, and U. Tariq, "Computer-aided deep learning model for identification of lymphoblast cell using microscopic leukocyte images," *Expert Systems*, p. e12894, 2021.
- [25] M. S. Hosseini, L. Chan, G. Tse, M. Tang, J. Deng, S. Norouzi, C. Rowsell, K. N. Plataniotis, and S. Damaskinos, "Atlas of Digital Pathology: A generalized hierarchical histological tissue type-annotated database for Deep Learning," in *Proc. of CVPR*, 2019.